UNCOVERING THE SPATIAL PATTERNS OF INVASIVE SPECIES VIA MACHINE LEARNING ON MULTI-TEMPORAL DRONE IMAGES

Hao Yuan Hung[1], Chin Rou Hsu[2], Bao Hua Shao[3], Nan Chang Lo[4], Kai Yi Huang[5]

[12] Dept. of Forestry, Chung-Hsing University, 145 Xingda Rd., Taichung 402, China Taipei,
Email: guava1128@gmail.com, 10230237bear@gmail.com
[3] Pu-Li Workstation, Nan-Tou Division Office, Forest Bureau, 124, Section 2, Zhongshan Road, Nantou 545, China Taipei,
Email: baobao357@gmail.com
[4] Experimental Forest Management Office, Chung-Hsing University, 145 Xingda Rd., Taichung 402, China Taipei,
Email: njl@nchu.edu.tw
[5] Dept. of Forestry, Chung-Hsing University, 145 Xingda Rd., Taichung 402, China Taipei,
Email: kyhuang@dragon.nchu.edu.tw

KEY WORDS: unmanned aerial vehicle (UAV), invasive alien plants (IAP), phenological traits, vegetation indices

ABSTRACT: Invasive alien plants (IAP) usually threaten the ecosystem of the invaded area. Because *in-situ* survey at a large-scale region with complex topography for IAPs is a daunting task, it is bound to rely on 3S technology for providing appropriate management strategies. Unmanned aerial vehicle (UAV) is critical to overcome above-mentioned difficulties; it can also make up for the shortcomings of the lack of mobility and autonomy in spaceborne/airborne systems. We used UAV to acquire images of *Spartina alterniflora* (smooth cordgrass, SC) and *Mikania micrantha* (bitter vine, BV) based on the critical dates in phenological cycles of them. We also included normalized difference vegetation index (NDVI) and green normalized difference vegetation index (GNDVI) to enhance vegetation features, in order to understand whether it can improve the classification accuracy. Maximum likelihood classifier (MLC), support vector machine (SVM), and random forest (RF) were used to perform species classification. The main results show that (1) UAV is sufficient to fully master the critical phenological traits of target species. (2) Multi-temporal images can promote the accuracy of classification. (3) The combination of NDVI, GNDVI with the pure spectra did not significantly improve the accuracy (4) The result of the second validation comparison of SC, the area estimated by SVM was the closest to the *in-situ* measured. In conclusion, we confirmed that UAV can precisely capture critical phenological traits of IAPs and more than enough to identify scattered IAPs. It is far more beneficial than done by spaceborne and airborne. Multi-temporal images can indeed promote the accuracy of the classification. The follow-up study will use UAV to obtain multi-temporal images to more accurately grasp phenology, and incorporate deep learning for perspective analysis. Not only estimate the distribution of IAPs but also return from the “metaverse” virtual Earth to the physical Earth for validation.

1. INTRODUCTION

Invasive alien plants (IAP) usually have a serious threat on the ecosystem of the invaded area. In recent years, under the background of transportation reform and globalization, frequent international trade and tourism have accelerated IAPs’ spread and lengthened their diffusion distance, which has become a universal ecological issue (Hulme, 2021). The IAPs that have invaded Taiwan Island for many years are widely distributed. They can be seen in green belts in the suburbs, and also in hills or inaccessible places. Nevertheless, *in-situ* survey at a large-scale region with complex topography for IAPs is a daunting task. Not only ones must be aware of potential hazards, but also it is hard to acquire sufficient on-site samples for species distribution modeling (SDM). Therefore, it is bound to rely on 3S technology for providing appropriate management strategies. Specifically, we must monitor large-scale vegetation with the contactless, macroscopic, dynamic, interdisciplinary, and high-efficiency advantages of remote sensing (RS) technology (Zeng *et al*., 2022). Then through the global navigation satellite system (GNSS) to obtain the precise location intelligence (LI), linking the digital Earth and the physical Earth, we can enter the geospatial information system (GIS) to accurately overlay various layers for integrated analysis.

Phenology is defined as the changes in life cycle of an organism. For plants, it includes germination, flowering, defoliation, fruiting with seasonal variations (Vilhar *et al.*, 2013; Warren *et al*., 2021). This will transform plants’ physiology or morphology i.e. appearance, and produce a unique spectral pattern as it transforms. Therefore, we can make good use of RS to capture this key, and use machine vision to automatically analyze the “appearance” in images. In this way, not only the physiological conditions of plants can be monitored, but also the spatial distribution potential of IAPs can be accurately grasped. Vegetation indices (VI) are the ratio between spectral bands from RS in terms of

plants that can be used to enhance the features of vegetation. They are one of the indicators for analyzing the phenology of plants and can be used to monitor vegetations (Zeng *et al.*, 2022).

IAPs are widely and fragmented patches in Taiwan Island. However, most studies on IAPs have been using moderate resolution spaceborne and airborne images. Subsequent analysis will be ineffective for the following reasons: (1) These two systems lack autonomy and mobility, so they cannot accurately grasp the characteristics of plants. In addition, the images are easily obscured by clouds, so they cannot correctly extract IAPs from surrounding plants. (2) The image resolution is insufficient, and the LI measured by GNSS is inaccurate. It is difficult to accurately calculate the distribution area of IAPs. In addition, matching with pixels is challenging. Not to mention how moderate resolution imagery can describe the finer details of narrow IAPs.

Recently, the burgeoning drone or unmanned aerial vehicle (UAV) has gradually become the mainstream of ecological investigation. As a vehicle, UAV offers unparalleled spatial and temporal resolution. Allow researchers to fly with higher flexibility. In view of this, we assessed the utility of multi-spectral UAV in sensing and mapping of two IAPs, *Spartina alterniflora* (smooth cordgrass, SC) and *Mikania micrantha* (bitter vine, BV), in central Taiwan Island. The UAV flight was based on the critical dates in phenological cycle of the two IAPs and acquired multi-temporal images to analyze their spatial distribution. The objectives of this study are to (1) Does UAV closely integrate the relationship between phenology and spectral pattern to correctly extract IAPs? (2) Does using VI improve classification accuracy? (3) From the quantitative data of area measurement, discuss the distribution area of SC estimated by each algorithm in "virtual Earth" and *in-situ* measured in "physical Earth", and compare the differences and the correct overlap rate.

2. STUDY AREA AND MATERIALS

2.1 Study Area

This study took two regions in central Taiwan Island as the study area. Yangs Tsu (YT) is located in Lukang Township, Changhua County at latitude 2,665,500 m to 2,665,750 m and longitude 192,250 m to 193,080 m, encompassing an approximate area of 20.75 ha (Fig. 1). YT is an intertidal close to the estuary with rich ecology; most of which are mudflats with extremely soft geology. It is also one of the areas with the largest SC population. At YT, we extrapolate to the whole area using the west plot. Another study area in Zhushan (ZS) Township, Nantou County at latitude 2,616,965 m to 2,617,070 m and longitude 217,070 m to 217,191 m, encompassing an approximate area of 1.27 ha (Fig. 1). ZS is a deserted open space with complex and steep terrain, many plants grow, and there may be a lot of BV. The land covers of YT and ZS were determined using UAV images and *in-situ* surveys data. All coordinate systems are TWD97 TM2.

2.2 Target species

Spartina alterniflora (smooth cordgrass, SC) is a perennial herb of the family Poaceae which is native to the salt marshes along the Atlantic coast of the Americas. Its rhizomes are well-developed and dense, which can penetrate deeply into the soil. SC has invaded Taiwan Island for more than ten years. Because of the strong fecundity and adaptability of SC, it forms a high-density single-species community in the intertidal zone, and has led to serious degradation to the ecosystem and biodiversity (Hwang, 2011; Yang, 2016; Tian *et al.*, 2020). SC has distinct phenological traits. The growth period is from April to October, and it will present a green appearance; from August to December, it will gradually wither and become brown (Fig. 2).

Mikania micrantha (bitter vine, BV) is a perennial creeper of the family Asteraceae which originates in South America. This species has long been known as a disrepute invader around the world (Holm *et al.*, 1977). BV often occurs in low-altitude areas, especially in abandoned tea plantation or orchard, abandoned farmland, betel palm orchards, artificial facilities or sewage ditches. Seriously, BV entangles or clings to other plants, preventing other plants from photosynthesizing, leading them to weakness and death. Due to the widespread of this species, there are harmful environmental and economic impacts. According to Kuo *et al*. (2002) observed the phenological traits of BV in Taiwan Island, its leaves unfold in early spring, and dry plants coexist with green leaves. Full of green leaves from June to October, similar to ordinary plants. It enters the flowering period in November and is full of white flowers; it withers in winter, and the plants are dry and tawny in January (Fig. 3). The white flowers in autumn and the tawny appearance in winter are the key to extracting BV from surrounding plants in summer.

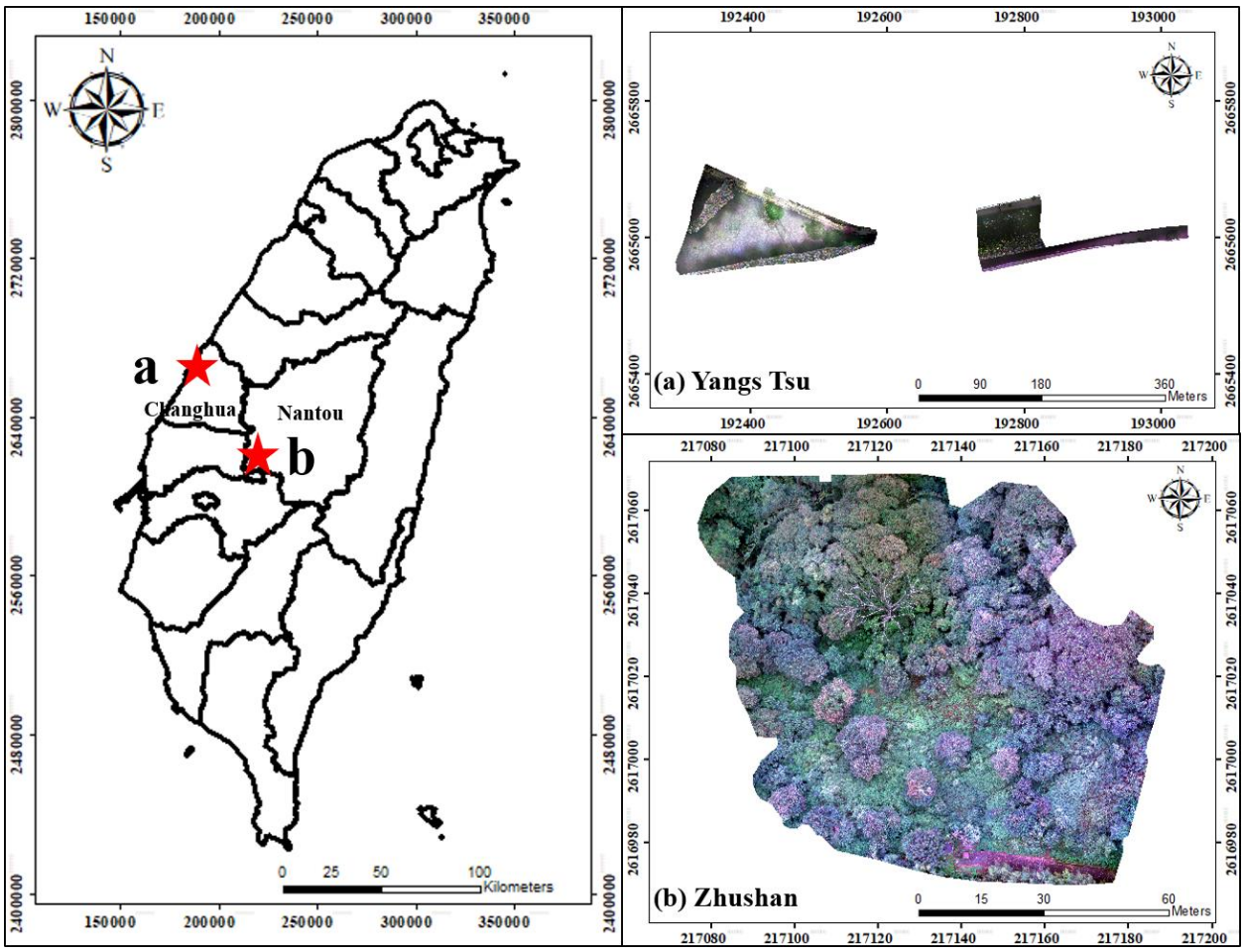

Figure 1. Study area: (a) Yangs Tsu and (b) Zhushan in central Taiwan Island.

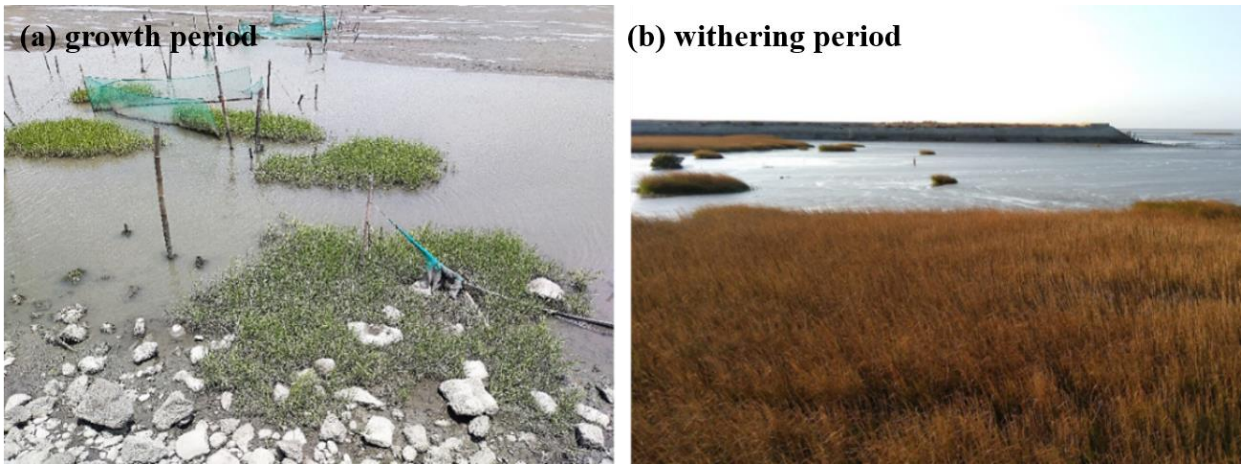

Figure 2. The phenological traits of SC.

Figure 3. The phenological traits of BV.

3. METHODS

3.1 UAV image acquisition

A DJI P4 Multispectral UAV (hereinafter referred to as P4M) was employed for acquiring IAPs color images. The sensing bands of the P4M are blue (450 ± 16 nm), green (560 ± 16 nm), red (650 ± 16 nm), red edge (730 ± 16 nm), and near-infrared (840 ± 26 nm). The images generated by the P4M are recorded in five bands with a 16-bit computer code scale (65,536), that is, the images generated by each band are divided into 65,536 gray levels from black to white (0–65,535). In addition, it is also equipped with real time kinematic (RTK) positioning function, shooting using the e-GNSS RTK positioning system provided by Center for Land Surveying and Mapping in Taiwan, through the wireless network to generate a virtual reference station (VRS), with RTK VRS for positioning.

UAV flight missions are performed based on the phenology of the two IAPs. At YT, we acquired bi-temporal images of SC on May 19 and November 7, 2021. At ZS, we acquired multi-temporal images of BV on January 27, April 6, August 23 and November 13 in 2021. The overlap rate of all missions remained at 80% / 70%; flying height remained at 30 m.

3.2 Field surveys

Even with the vast amount of data available with UAVs, we still need ground survey data. However, measurements in the intertidal zone or in the mountains cannot be carried out by means of transportation, but can only on foot. We used the Trimble R12 GNSS receiver to measure the area of one of the SC communities, and measure the coordinates of the ground control points (GCP) and check points before the flight missions. Using the LI as a bridge, we closely combine “air” and “ground”. In this way, we can enter the metaverse “virtual Earth” for analysis and modeling “physical Earth.”

3.3 Data Preprocessing

First, the original image taken by UAV needs to undergo orthographic corrections. We used Pix4Dmapper based on the TWD97 TM2 coordinate system to perform coordinate transformation and mosaic multiple images to produce orthorimages, and import GCPs to correct positioning errors in the process. Second, this study also used Erdas IMAGINE image processing software to perform relative radiation correction with histogram matching (HM) method to eliminate the problem that the reflection value is different from the actual value caused by the change of the external illumination angle and the sensor itself. Furthermore, we used ArcGIS 10.3 to combine different phenological images of SC and BV. It is helpful to know the most critical phenological events.

3.4 Vegetation indices (VI)

Tucker *et al*. (1979) were the first to use normalized difference vegetation index (NDVI) to measure green plant biomass. It is the most commonly used VI in RS. NDVI is able to monitor changes in vegetation, mainly using the difference between the near-infrared (NIR) channel and the red channel. The value of NDVI is between -1 and 1, and the closer to 1, the more vegetation cover. Its equation is defined by:

$$NDVI = (NIR - Red)/(NIR + Red) \quad (1)$$

Compared with NDVI, green normalized difference vegetation index (GNDVI) is more sensitive to chlorophyll. It uses green channel instead of red channel. Like NDVI, GNDVI values range from -1 to 1. Because the saturation point is higher than NDVI, it can make up for the problem of its saturation. As for how to calculate GNDVI, the equation is as follows (Gitelson *et al.,* 1996):

$$GNDVI = (NIR - Green)/(NIR + Green) \quad (2)$$

We calculated these two VIs with the raster calculator in ArcGIS and classified them with every pure spectra and combined images.

3.5 Image classification

This study selected training samples and classify them based on the field survey data and orthoimages. YT can be classified as SC, mudflat, herbs (evergreen), road, river. ZS can be classified as BV, hardwood, herbs and ferns, road, litter or soil, bamboo. Then we reclassified them as SC, non-SC; BV, and non-BV. Then, maximum likelihood classifier (MLC), support vector machine (SVM), and random forest (RF) were used to perform IAPs recognition and classification.

We take MLC as the traditional supervised classification algorithm, and SVM is implemented in ENVI 5.3, both with default settings. SVM adopts One-Against-One method in ENVI 5.3, and we will try to test One-Against-All and adjust its “gamma” parameter and “cost” parameter in the future. We tuned the hyperparameters of RF. The “maximum depth” was set to 5; “minimum samples split” was 30; and “minimum samples leaf” was 15.

3.6 Assessing classification accuracy

We used the split-sample validation approach to extract 1,000 samples from each training sample by stratified random sampling, and then selected 2,000 samples from a completely independent test sample for validation. This choice is reasonable as it represents a typical condition of real operational applications (Dalponte *et al*., 2008), i.e., spatial extrapolation to a large area with a small amount of training data. We used the *kappa* coefficient of agreement and overall accuracy (OA) as accuracy evaluation indicators.

4. RESULTS AND DISCUSSION

4.1 Gray-level values in two IAPs

This study found that SC has a “plant” spectral pattern during the growth period in May, and a similar “soil” spectral pattern during the withering period in November. The red band reflection of the former is significantly lower than that of the latter, forming a “trough” zone; the NIR band reflection of the former is significantly higher than that of the latter, forming a “plateau” zone relatively (Fig. 4a).

When BV was full of clusters of white flowers in November, the gray level values in the five bands was significantly

higher than the spectral pattern of “plant” and “soil” in the other three months (Fig. 4b). The spectral pattern of this phenological feature can clearly extract the "main" target species from the surrounding plants (especially herbs and ferns) in the same period, highlighting the critical identification effect of this phenology. Therefore, this study first demonstrate that UAV is sufficient to fully master the critical phenological traits of target species.

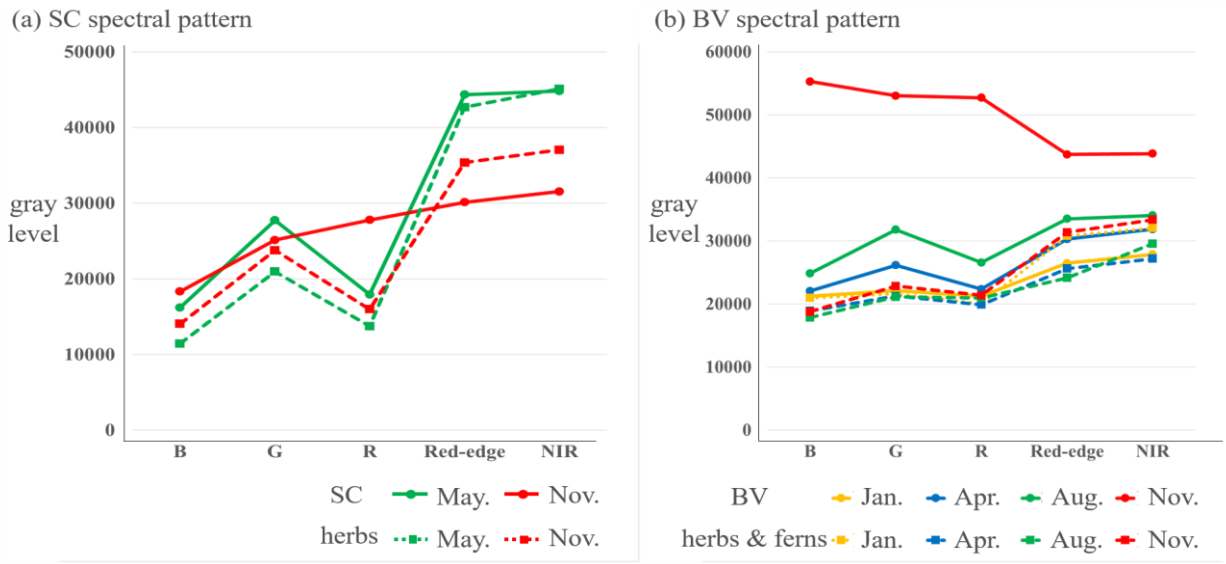

Figure 4. Line chart of the average gray-scale values of the two IAPs in different phenological periods.

4.2 Image classification results

For classification, the use of multi-temporal images with critical phenology could reduce confusion. The classification results of the three algorithms applied in YT prediction are shown in Table 1. Using single-temporal image of the growth period had lower accuracy due to SC confusion with herbs. The single-temporal image in the withering period could distinguish evergreen herbs and SC, which improved the accuracy, but there was still confusion between SC and mudflat. When used bi-temporal images, the *kappa* value and OA of the three algorithms were significantly improved compared with those using only single-temporal images. Among them, the first two values of SVM were the highest, and the improvement was also more. Its *kappa* value was increased by 30%, and OA was increased by 24%. However, the two evaluation values of the three algorithms were less than 0.85, which was mainly due to the confusion of mudflat, road and river extrapolated from another plot.

Table 1. Classification accuracy of SC from single-temporal and bi-temporal images.

	MLC		SVM		RF	
	kappa	OA	*kappa*	OA	*kappa*	OA
growth period (5/19)	0.52	0.62	**0.48**	**0.58**	0.63	0.70
withering period (11/7)	0.63	0.71	0.64	0.71	0.71	0.76
bi-temporal (5/19, 11/7)	0.75	0.80	**0.78**	**0.82**	0.76	0.81

As for the classification results of BV, it was found that the images in the withering period could distinguish the surrounding evergreen plants. The green leaves period could distinguish artificial facilities due to the characteristics of plant spectral pattern, but it was easy to be confused with the surrounding herbs. The images in puberty could distinguish almost all classes because of the particularly obvious white flowers. The classification results of the three algorithms in different combinations of images are listed in Table 2. The use of bi-temporal images improved slightly, while the third-phase images greatly improved the classification accuracy, *kappa* value was increased by 49%, and OA was increased by 41%. However, after the images of the full flowering period in November were added to each combination, the two indicators improved most significantly. It highlights the importance of full-flowering images in the extraction of BV.

Table 2. Classification accuracy of BV from each image combination.

	MLC		SVM		RF	
	kappa	OA	*kappa*	OA	*kappa*	OA
single-temporal (1)	0.36	0.47	0.35	0.46	0.65	0.71
single-temporal (4)	0.37	0.48	**0.34**	**0.45**	0.64	0.70
single-temporal (8)	0.55	0.62	0.55	0.62	0.72	0.77
single-temporal (11)	0.72	0.76	0.73	0.78	0.79	0.82
bi-temporal (1, 4)	0.52	0.60	0.47	0.56	0.68	0.73
bi-temporal (1, 8)	0.59	0.66	0.60	0.67	0.72	0.77
bi-temporal (1, 11)	0.78	0.81	0.77	0.81	0.81	0.84
bi-temporal (4, 8)	0.61	0.68	0.62	0.68	0.73	0.77
bi-temporal (4, 11)	0.74	0.78	0.75	0.79	0.80	0.84
bi-temporal (8, 11)	0.81	0.84	0.82	0.84	0.81	0.84
three-temporal (1, 4, 8)	0.62	0.69	0.66	0.72	0.73	0.78
three-temporal (1, 4, 11)	0.78	0.82	0.77	0.81	0.82	0.85
three-temporal (1, 8, 11)	0.76	0.80	0.81	0.84	0.81	0.84
three-temporal (4, 8, 11)	0.81	0.84	**0.83**	**0.86**	0.82	0.85
four-temporal (1, 4, 8, 11)	0.80	0.83	0.82	0.85	0.82	0.85

***** Numbers in the table represent months

Since the improvement of SVM was the most obvious, we continued to use it to discuss the results. Thematic maps of SC and BV shown in Figure 5 and Figure 6. Compared with UAV images, using only single-temporal images, both IAPs were misclassified. When SC used bi-temporal images, the situation of omission could be significantly improved (Fig. 5). BV was largely confused with the surrounding herbs in the single-temporal image in April; there was a slight improvement using the bi-temporal image. When adding a November image full of white flowers, the aforementioned problem was greatly improved (Fig. 6). It is crucial to show the November images again.

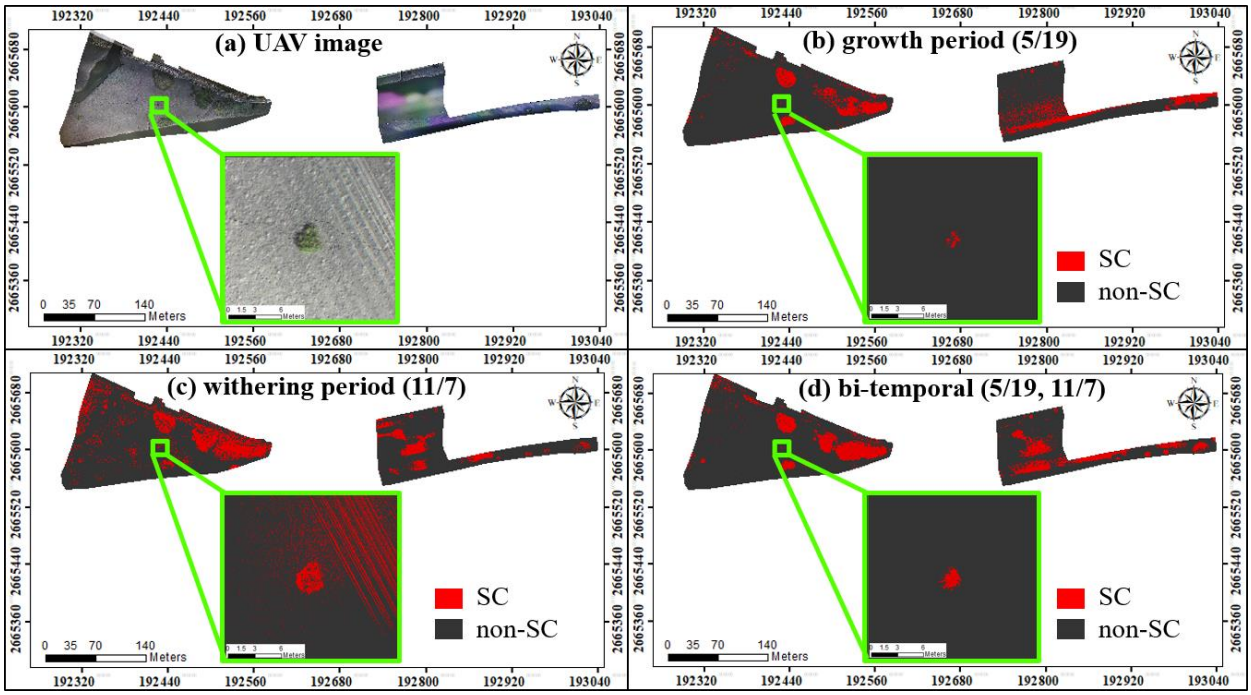

Figure 5. SC thematic map (take SVM as an example).

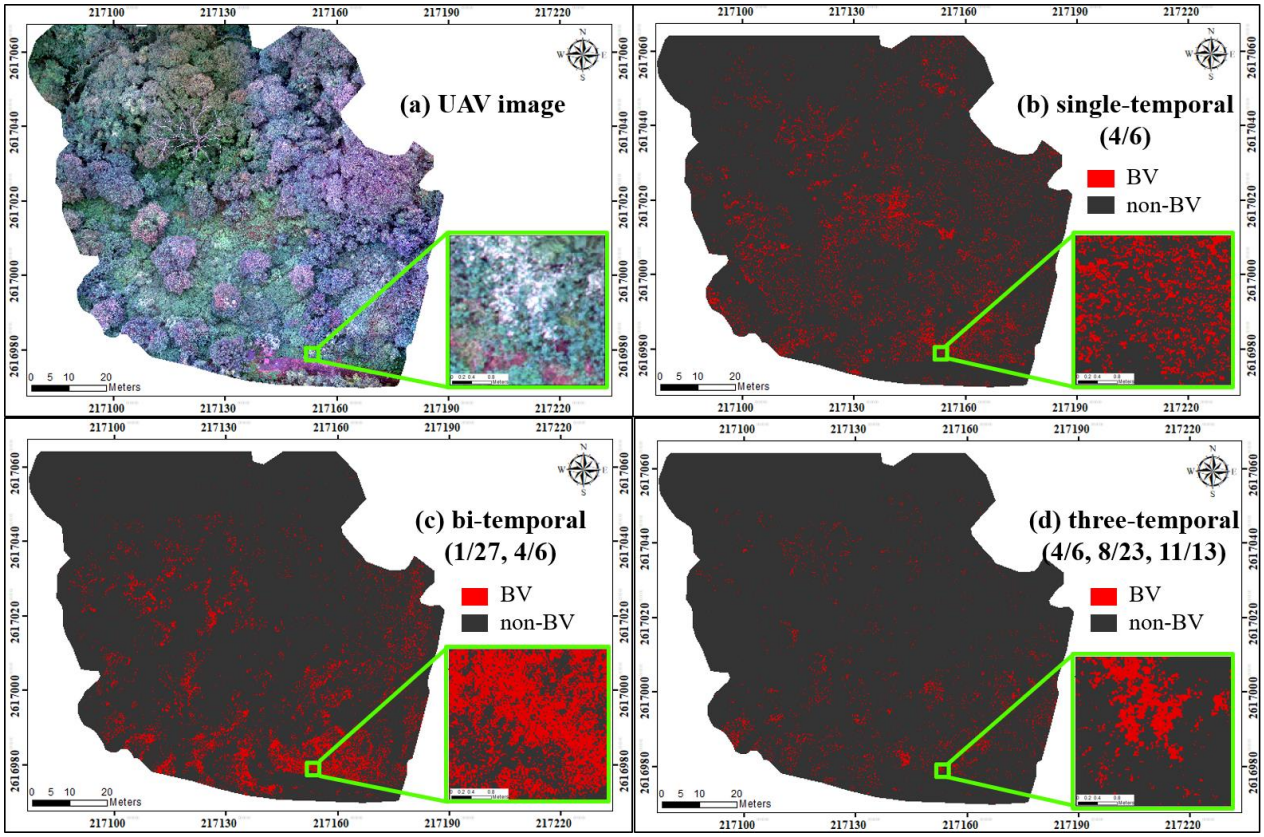

Figure 6. BV thematic map (take SVM as an example).

4.3 Classification results of pure spectra combined with VIs

Since the results of the SVM were the best in the previous paragraph, this paragraph will discuss the results of the classification for SVM. The classification accuracy of pure spectrum, superimposed NDVI, and GNDVI of different phenological combinations of the two IAPs is shown in Table 3 and Table 4. The combination of VI with the pure spectra did not significantly improve the accuracy, and *kappa* values were only about ±1–3% than that of the pure spectra. We think it is probably because: (1) Most of ground cover in ZS is vegetation, so that the VI of BV is not much different from that of other plants. (2) Our grasp of phenology was not sufficient, and SC was not all in a state of withering. (3) Because plant physiology is not static, but dynamic, and will respond differently to climates.

Table 3. Influence of VIs on SC classification accuracy (take SVM as an example)

date	Pure spectra		Pure spectra + NDVI		Pure spectra + GNDVI	
	kappa	OA	*kappa*	OA	*kappa*	OA
growth period (5/19)	0.48	0.58	0.46	0.57	0.46	0.57
withering period (11/7)	0.64	0.71	0.63	0.70	0.63	0.70
bi-temporal (5/19, 11/7)	0.78	0.82	0.77	0.81	0.77	0.81

Table 4. Influence of VIs on BV classification accuracy (take SVM as an example)

	Pure spectra		Pure spectra + NDVI		Pure spectra + GNDVI	
	kappa	OA	*kappa*	OA	*kappa*	OA
single-temporal (1)	0.35	0.46	0.33	0.45	0.32	0.43
single-temporal (4)	0.34	0.45	0.37	0.48	0.37	0.48
single-temporal (8)	0.55	0.62	0.55	0.62	0.55	0.62
single-temporal (11)	0.73	0.78	0.73	0.78	0.73	0.78
bi-temporal (1, 4)	0.47	0.56	0.36	0.46	0.32	0.44
bi-temporal (1, 8)	0.60	0.67	0.60	0.66	0.60	0.67
bi-temporal (1, 11)	0.77	0.81	0.77	0.81	0.78	0.82
bi-temporal (4, 8)	0.62	0.68	0.62	0.68	0.62	0.68
bi-temporal (4, 11)	0.75	0.79	0.77	0.81	0.77	0.81
bi-temporal (8, 11)	0.82	0.84	0.82	0.84	0.82	0.84
three-temporal (1, 4, 8)	0.66	0.72	0.60	0.66	0.60	0.66
three-temporal (1, 4, 11)	0.77	0.81	0.78	0.81	0.32	0.44
three-temporal (1, 8, 11)	0.81	0.84	0.83	0.86	0.83	0.86
three-temporal (4, 8, 11)	0.83	0.86	0.83	0.86	0.83	0.86
four-temporal (1, 4, 8, 11)	0.82	0.85	0.82	0.86	0.82	0.86

***** Numbers in the table represent months

4.4 Second validation

The data modeling in the "virtual Earth" must be returned to the "physical Earth" to verify whether it matches. The second validation of BV has not been done in this study because of insufficient manpower and time allocation, and the distribution of BV is too widespread and scattered. We will be supplemented in follow-up study. As for the results of the second validation of a community of SC, the difference between the SVM and the physical was the smallest. The difference was only 0.006 ha from the *in-situ* measured value, and the correct overlap rate reached 71.73%. A possible reason for this result was that the leaf of SC extended to the embankment slope, which was identified by algorithms, but it was difficult to position this area *in-situ*.

Table 5. The results of second validation.

algorithms	estimated area (ha)	difference from the measured value (ha)	Correct overlap rate (%)
MLC	0.017	0.007	63.54%
SVM	0.018	0.006	71.83%
RF	0.015	0.009	57.62%
measured value	0.024	-	-

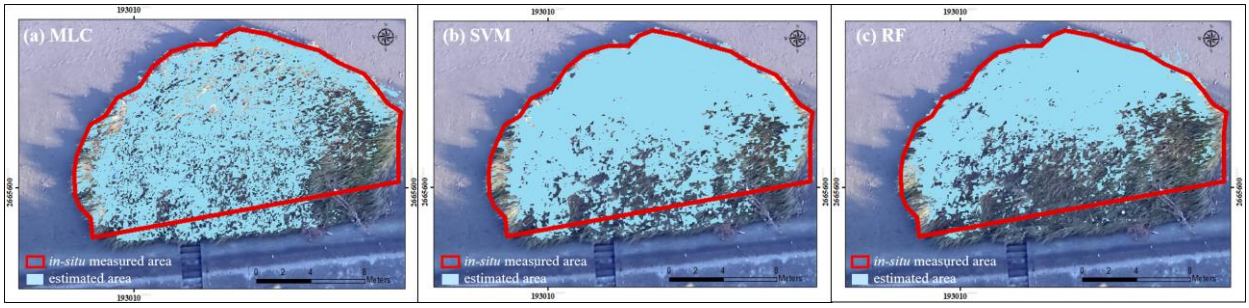

Figure 7. Comparison of estimated values and *in-situ* measured.

5. CONCLUTIONS

In this study, UAV was used to obtain large-scale IAPs data, and Trimble R12 was used to measure LI with high accuracy, and it traveled between the "metaverse" virtual Earth and the "physical Earth". First, we confirmed that the high autonomy and mobility of UAV can precisely capture the phenological traits of plants and more than enough to identify scattered IAPs. It is far more beneficial than done by spaceborne and airborne. Especially in the difficult intertidal zone or mountainous with complex topography, we need to use UAV to cross the environmental barrier. Using multi-temporal images do significantly improve classification accuracy. However, the addition of two VIs did not improve the accuracy significantly, which may be related to the fact that the study area is all plants, and the

phenological traits have not been fully grasped.

In terms of future developments of this paper, we are planning to: (1) As “Rome was not built in a day,” we will take advantage of the highly autonomous and mobility of UAV to capture multi-temporal images from growth period, puberty to withering period (first year 8–12 periods), and even monitoring across the years to find the best combination of phenological traits of IAPs, and gain insight into the most critical date images. (2) If we can obtain a heavy UAV, we will use it as a priority for the expanded survey scale; if not, it will be paired with appropriate satellite/aerial images. (3) rely on UAV to obtain huge “light pattern” information, using deep learning for perspective analysis. (4) Sampling to *in-situ* measure the coverage area of IAPs, and compare it with the estimated results of the “virtual Earth” i.e., calculate the root mean square error between *in-situ* measured values and estimated values. Not only estimate the distribution of IAPs’ high potential but also return from the “metaverse” virtual Earth to the physical Earth for validation. Another point that cannot be ignored is to confirm how serious the impact of IAPs on Taiwan Island’s ecosystem is. We will use 3S technology to analyze and confirm the severity of the damage in the future.

6. REFERENCES

Dalponte, M., Bruzzone, L., and Gianelle, D., 2008. Fusion of hyperspectral and LIDAR remote sensing data for classification of complex forest areas. IEEE Trans. Geosci. Remote Sens., 46 (5), pp. 1416-1427.

Gitelson, A.A, Kaufman, Y.J., Merzlyak, M.N., 1996. Use of a green channel in remote sensing of global vegetation from EOS-MODIS. Remote Sensing of Environment, 58 (3), pp. 289-298.

Holm, L.G., Plucknett, D.L., Pancho, J.V., Herberge, J.P., 1977. The World’s worst weeds: distribution and biology. University Press of Hawaii, Honolulu.

Hulme, P.E., 2021. Unwelcome exchange: International trade as a direct and indirect driver of biological invasions worldwide. One Earth, 4 (5), pp. 666-679.

Hwang, C.C., 2011. A new exotic invader to taiwan’s coastal marsh. Nature conservation quarterly, (74), pp. 36-40.

Kuo, Y.L., Chen, T.Y., Lin, C.C., 2002. Using a Consecutive-Cutting Method and Allelopathy to Control the Invasive Vine, *Mikania micrantha* H.B.K. Taiwan Journal of Forest Science, 17 (2), pp.171-181.

Tian, J., Wang, L., Yin, D., Li, X., Diao, C., Gong, H., Shi, C. Menenti, M., Ge, Y., Nie, S., Ou, Y., Song, X., and Liu, X., 2020. Development of spectral-phenological features for deep learning to understand Spartina alterniflora invasion. Remote Sensing of Environment, 242, 111745.

Tucker, C.J.,1977. Red and photographic infrared linear combinations for monitoring vegetation. Remote Sensing of Environment, 8 (2), pp. 127-150.

Vilhar, U., Beuker, E., Mizunuma, T., Skudnik, M., Lebourgeois, F., Soudani, K., and Wilkinson, M., 2013. Tree phenology. Developments in Environmental Science, 12, pp. 169-182.

Warren, R., Price, J., and Jenkins, R., 2021. Climate change and terrestrial biodiversity. In: The Impacts of Climate Change, edited by Letcher, T.M., Elsevier, pp.95-97.

Yang, L., 2016. Alternative management strategies for the coastal wetlands invaded by exotic species of *Spartina alterniflora*. Journal of Wetlands, 5 (1), pp. 40-54.

Zeng, J., Sun, Y., Cao, P., Wang, H., 2022. A phenology-based vegetation index classification (PVC) algorithm for coastal salt marshes using Landsat 8 images. International Journal of Applied Earth Observation and Geoinformation, 110, 102776.